International Scientific Colloquium
Modelling for Electromagnetic Processing
Hannover, October 27-29, 2008

TMF's in Crystal Growth and Solidification of Semiconductors, Oxides and Fluorides

N. Dropka, Ch. Frank-Rotsch, W. Miller, U. Rehse, P. Rudolph

Abstract

Travelling magnet fields (TMF's) have be shown to be a powerful tool to influence the melt convection in crystal growth processes. In this paper we present the results of a systematic study on the influence of a TMF on the solid/melt interface for different materials in the same kind of environment.

Introduction

Travelling magnet fields (TMF's) can be used to influence the melt convection in different ways: damping temperature oscillations [1], smooting the melt/solid interface [2], increasing the mixing [3] and others. In order to get high Lorentz forces in the melt by using low power input a modified resistent heater is used as the generator of the electro-magnet field [4]. In this paper we present the results of a systematic study on the influence of a TMF on the solid/melt interface for different materials in the same kind of environment. For this purpose we choose a typical furnace used for the vertical gradient freeze (VGF) method of crystal growth. In a VGF furnace Ge crystals has been successfully grown with a heater-magnet module [5]. The parameters for the TMF in order to obtain an almost flat interface have been evaluated by means of axi-symmetric numerical calculations [2]. In this paper we present the results of axi-symmetric numerical calculations with the software package CrysMAS[6] to show the influence of different TMF's on the melt convection rather than to optimize process. In particular, we have performed calculations for Ge, Si, and BaF_2.

1. Calculations

We use a typical VGF configuration (see Fig. 1), where the ampoule (diameter: 113 mm) is half filled by already crystallized material. The top and bottom resistance heaters are only for heating, whereas the three side heaters are used both for heating and producing a TMF. The phase shift in the side heaters is counted from top to bottom. The software package CrysMAS[6] was used to perform the following steps:

1. Calculation of temperature field without melt convection and fixed interface.
   Adjusting power of heaters.
2. Calculation of buoyancy convection and interface shape.
   Taking the heater power from step 1.
3. Calculation of buoyancy and forced convection caused by Lorentz forces.

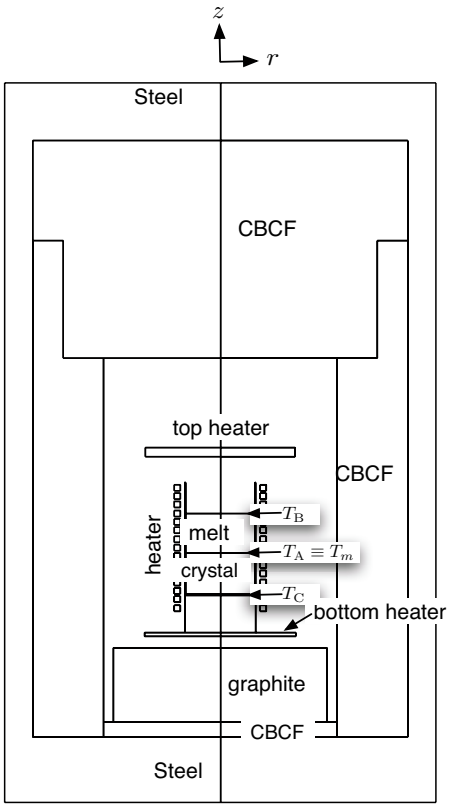

Figure 1: VGF furnace for computations.

In order to have the same relation of heat flux through the melt and through the isolation we set the heat conduction of the latter according to:

$$\lambda^{\text{iso}} = \lambda^{\text{CBCF}} \frac{\lambda^X_{\text{melt}}}{\lambda^{\text{Ge}}_{\text{melt}}}. \tag{1}$$

λ^{CBCF} is the heat conductivity of the original material (CBCF), λ^X_{melt} is the heat conductivity of material X in the melt.

In step 1 the heater power was adjusted so that there is the melting-point temperature T_m at point A and $T_m + 10$ K at point B (see Fig. 1). For point C a temperature of $T_{\text{C}} = T_m - 40$ K was achieved for Ge. We consider the heat fluxes through melt and crystal defined by the temperatures T_{A}, T_{B}, and T_{C}: $J^{\text{Ge}}_{\text{melt}} = \lambda^{\text{Ge}}_{\text{melt}}(T_{\text{B}} - T_{\text{A}})/h_{\text{melt}}$ and $J^{\text{Ge}}_{\text{solid}} = \lambda^{\text{Ge}}_{\text{solid}}(T_{\text{A}} - T_{\text{C}})/h_{\text{solid}}$, respectively. The heights of the melt h_{melt} and the solid h_{solid} are the same (64mm). For the other materials we use the same relation of the heat fluxes $J^{\text{Ge}}_{\text{solid}}/J^{\text{Ge}}_{\text{melt}}$ and adjust the power of the heaters in order to get

$$T^X_{\text{C}} = T^X_m - 40\text{ K}\,\frac{\lambda^X_{\text{melt}}}{\lambda^{\text{Ge}}_{\text{melt}}}\frac{\lambda^{\text{Ge}}_{\text{solid}}}{\lambda^X_{\text{solid}}}, \tag{2}$$

where λ^X_{solid} is heat conductivity of material X for the solid. From the calculated temperature field ΔT in Table 1 was computed as the radial temperature on the melt surface, which is largest radial one in the melt.

	λ_{melt}	λ_{solid}	L	σ_{el}	ν	α	ρ_{melt}	ΔT	F_{buoy}
	W/(mK)		Jm^{-3}	S/m	m^2/s	K^{-1}	kg m^{-3}	K	Nm^{-3}
Ge	39.0	17	4.0×10^9	1.7×10^6	1.4×10^{-7}	1.1×10^{-4}	5500	2 K	11
Si	67.0	22	4.6×10^9	1.2×10^6	3.4×10^{-7}	1.5×10^{-4}	2530	7 K	26
BaF_2	0.2	2.0	1.83×10^9	3.9×10^2	2.5×10^{-6}	2.0×10^{-5}	4830	-	-

Table 1: Table of material parameters. The temperature difference ΔT is defined by the difference of temperatures on the melt surface at the center and the rim.

In step 2 the heater powers of step 1 were used and the growth velocity was set to $v_{\text{growth}} = 3\ \text{mm/h}$ for Ge. For the other materials the growth velocity was obtained from:

$$v^X_{\text{growth}} = v^{\text{Ge}}_{\text{growth}} \frac{L^{\text{Ge}}}{L^X}, \tag{3}$$

where L^X is the latent heat of material X.

We have performed runs for Ge, Si, and BaF_2. The latter has a much smaller thermal conductivity than the others (see Table 1). It was not possible to get a reasonable temperature field with the furnace configuration shown in Fig. 1. Therefore, for BaF_2 we calculated Lorentz forces only.

The computations for TMF's were done with a variation in the phase shifts ($\phi = \pm 30^o, \pm 60^o, \pm 120^o$) of the three heater segments and the frequency (20 Hz, 50 Hz, 200 Hz, 500 Hz). So, in total we have performed 24 calculations with TMF for every material.

In order to apply the same order of Lorentz forces for the different materials we take the electrical current in the case of material x according to:

$$I^X = I^{\mathrm{Ge}} \sqrt{\frac{\sigma_{\mathrm{el}}^{\mathrm{Ge}}}{\sigma_{\mathrm{el}}^{X}}}. \qquad (4)$$

Here σ^X is the electrical conductivity of material X. For Ge we used 100 A, which gives Lorentz force densities larger than the estimated buouyancy force densities (see Table 1).

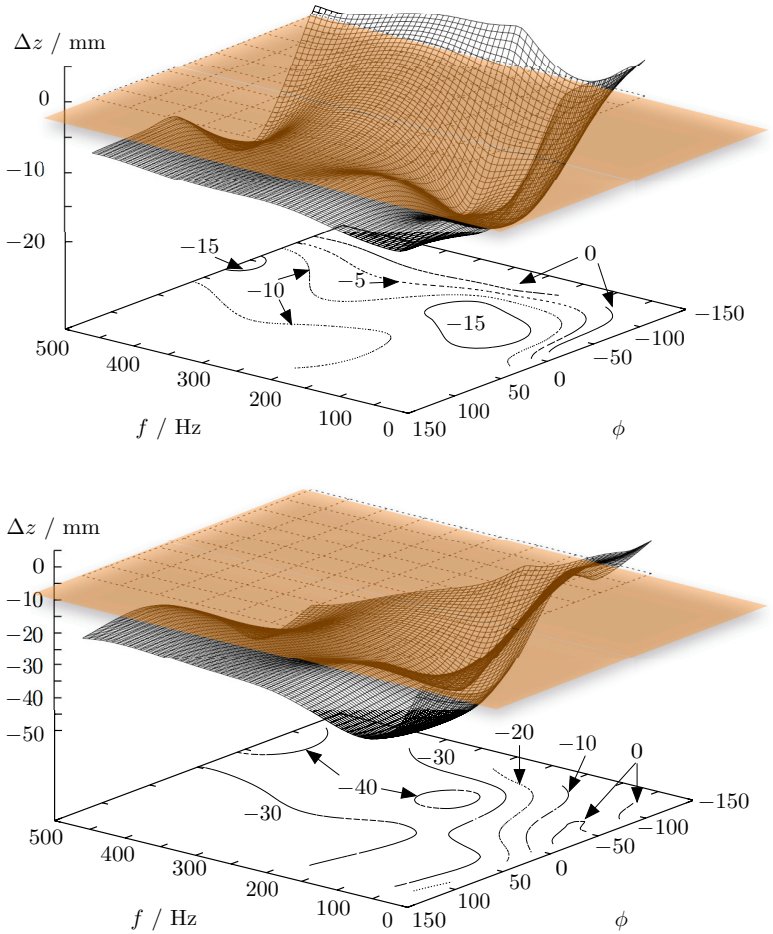

Figure 2: Deflection Δz for the interface for Ge (top) and Si (bottom) as a function of the frequency f and the phase shift ϕ. For comparison the deflection in the case of buoyancy flow only is shown as a plane. Isolines of Δz are plotted on the bottom plane.

2. Results

For Ge and Si we have obtained the temperature field and the shape of the solid/melt interface. The Lorentz force densities are always larger than the estimated buoyancy force densities, even for the lowest frequency $f = 20$ Hz. Therefore, the forced convection is dominating. This is of advantage for a good mixing but it is not optimal for getting a flat interface. However, the thermal optimization of the furnace was not subject of investigation, because it should be done according to the material to be crystallized.

Firstly, we compare the results for Ge and Si, which have similiar physical properties (see Table 1). In Figure 2 the deflection of the interface is shown, where Δz is measured at the axis. If there is buoyancy convection only the interface is slighlty concave in the case of Ge ($\Delta z = -1$ mm) and more concave in the case of Si ($\Delta z = -6$ mm). For most parameters of the

TMF the induced convection rolls enhance the concavity of the interface. A positiv deflection ($\Delta z > 0$) is obtained for the smallest frequency ($f = 20$ Hz) both for Ge and Si. Unfortunately, the interface is concave in the vicinity of the three phase junction (melt/crystal/crucible) as shown in Figure 3.

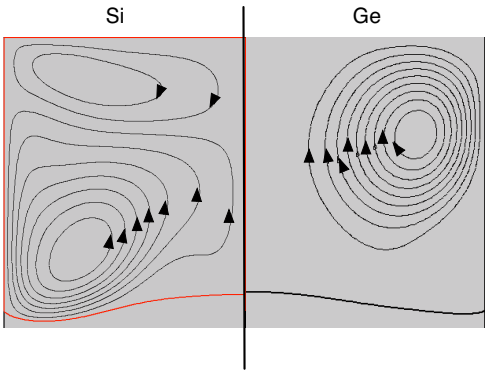

Figure 3: Streamlines and interface shapes for Si and Ge, presented left and right of the symmetry axis ($f = 20$ Hz, $\phi = -120^o$).

As already mentioned no proper thermal conditions could be achieved for BaF_2. Here we compare Lorentz forces only. Firstly, we address the question if setting the electrical current according to Eq. 4 leads to the same order of magnitude of Lorentz force densitites. In Figures 4 and 5 we show minima and maxima of F_r and F_z for all three materials in the case of $\phi = 30^o$, respectively. Ge and Si give very similar results whereas BaF_2 with its much smaller electrical conductivity exhibits some differences. Concerning F_r, the maximum F_r directing towards the axis ($F_r < 0$) is very small compared to Si and Ge. On the other hand there regions in BaF_2 melt, where the Lorentz force is directing outwards ($F_r > 0$), which does not occur in the case of Si and Ge. The maximum of F_r for Ge and Si is zero (see Figure 4). The positive F_r in the case of BaF_2 is induced near the melt surface, where the upper and middle inductors meet.

F_z is about the same for all materials up to $f = 50$ Hz but for larger frequencies F_z becomes negativ near the melt surface for Ge and Si (actually the same region, where F_r becomes positiv for BaF_2) and the (positiv) maximum is about double the one in the case of BaF_2 (see Figure 5). For a more detailed look on the force density field we chose the runs for $f = 50$ Hz (and $\phi = 30^o$). In Figure 6 we show the F_z field for Si and Ge, which looks very similar. For BaF_2 the maximum F_z is in the same range as for the other two materials but the distribution is quite different. In addition, the required electrical current is rather high: $I = 6585$ A. Such a high electrical current is not useful from a practical point of view. As we saw from Figures 4 and 5 the maximum of the Lorentz force densities increases with increasing frequencies. For BaF_2 we chose $f = 15$ kHz and reduced the current to $I = 750$ A, which is in the range used in crystal growth of such material. The resulting Lorentz force densities F_z are shown on the right hand side of Figure 7.

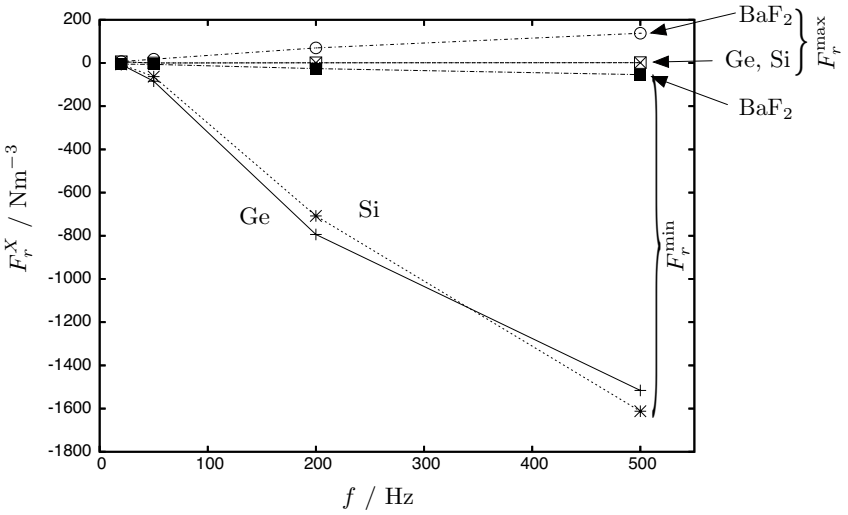

Figure 4: Minima ($F_r^{\min}$) and maxima ($F_r^{\max}$) of the radial component F_r of the Lorentz force density as a function of the applied frequency f for all three materials investigated.

There is not much difference between field distribution of F_z for low frequency and high current and that for high frequency and low current.

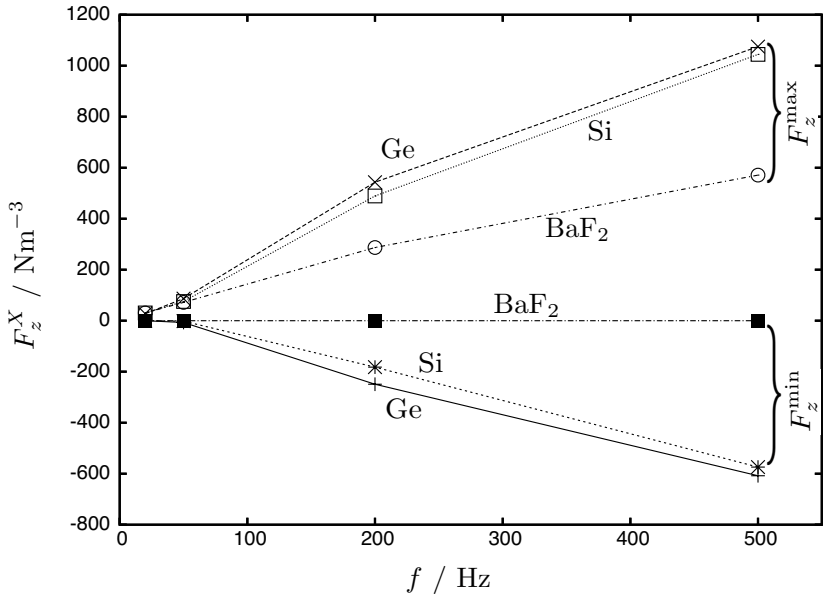

Figure 5: Minima ($F_z^{\min}$) and maxima ($F_z^{\max}$) of the vertical component of the Lorentz force density F_z as a function of the applied frequency f for all three materials investigated.

We did not yet discuss the penetration of the electro-magnetic field into the melt. For $f = 50$ Hz the skin depth is $\delta = 55$ mm for the material with highest electrical conductivity (Ge). This of the order of the radius of the crucible. For the next frequency computed ($f = 200$ Hz) the skin depth is only half of that at $f = 50$ Hz and the field is significantly reduced in the melt. Because of its small electrical conductivity the skin depth for BaF_2 is very large in all cases, even for $f = 15$ kHz we have $\delta = 210$ mm. The different skin depth might be the reason for the different results for F_r and F_z at $f = 200$ Hz and $f = 500$ Hz.

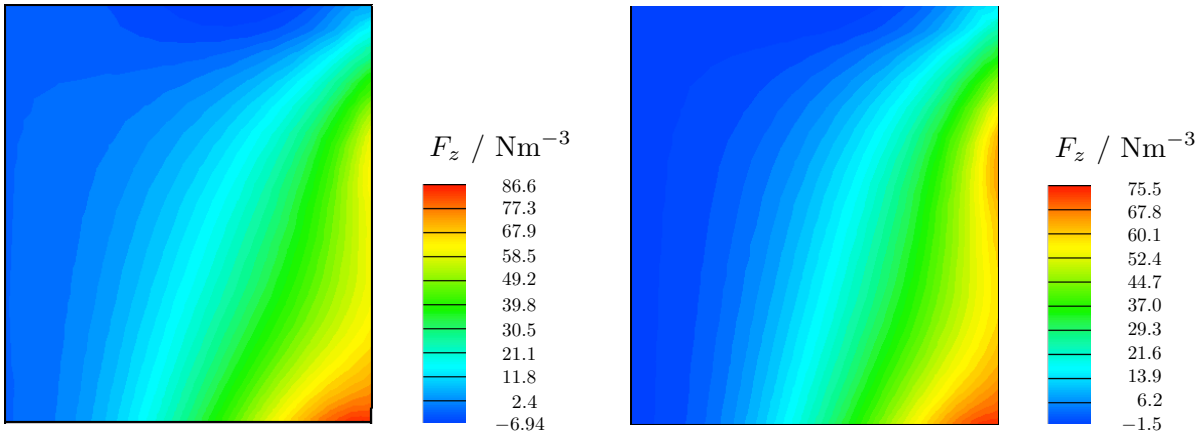

Figure 6: Vertical component of the Lorentz force densities for $f = 50$ Hz and $\phi = 30°$. Left: Ge. Right: Si.

Conclusions

We have performed global calculations of the temperature field, the Lorentz forces, the melt convection, and the melt/solid interface for a set of TMF's with different phase shifts and frequencies using the software package CrysMas. Also for materials with small conductivity Lorentz force densities comparable or larger than the buoyancy force densities can be achieved

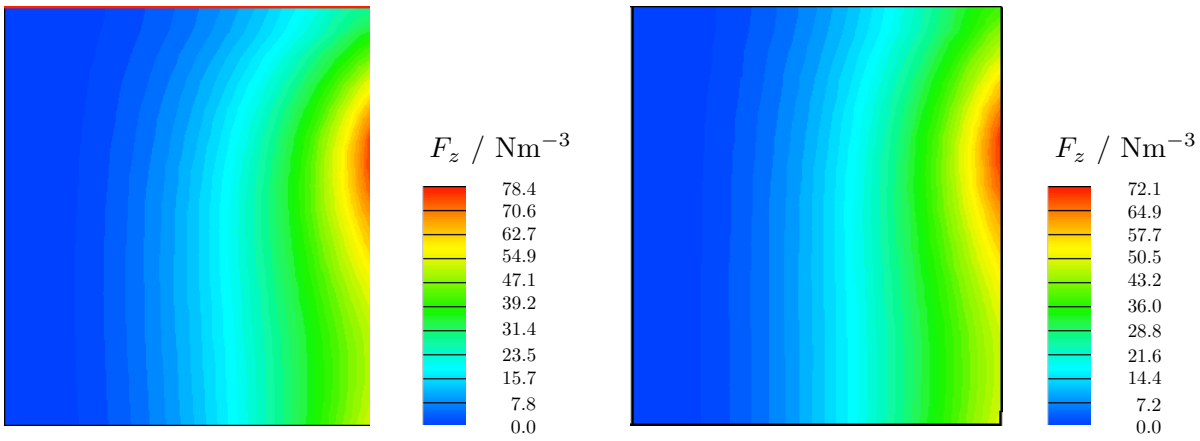

Figure 7: Vertical component of the Lorentz force densities for BaF_2 and a phase shift of $\phi = 30^o$. Left: An electrical current of $I = 6585$ A and $f = 50$ Hz was applied. Right: An electrical current of $I = 750$ A and $f = 15$ kHz was applied.

by using moderate electrical currents. For such materials high frequencies should be chosen.

For crystal growth the thermal field defined by heating and isolation is the most important point. A TMF can be used to optimize the process further by flatening the interface and better mixing of the melt. The AC current needed for the TMF can be accomplished bei a DC current in order to meet the required total current for the heating.

References

[1] O. Klein, C. Lechner, P.-E. Druet, P. Philip, J. Sprekels, C. Frank-Rotsch, F.-M. Kießling, W. Miller, U. Rehse, and P. Rudolph, *Numerical simulation of Czochralski crystal growth under the influence of a traveling magnetic field generated by an internal heater-magnet module (HMM)*, J. Crystal Growth **310** (2008), pp. 1523–1532.

[2] C. Frank-Rotsch, D. Jockel, M. Ziem, and P. Rudolph, *Numerical optimization of the interface shape at the VGF growth of semiconductor crystals in a traveling magnetic field*, J. Crystal Growth **310** (2008), pp. 1505–1510.

[3] A. Cramer, S. Eckert, V. Galindo, G. Gerbeth, B. Willers, and W. Witke, *Liquid metal model experiments on casting and solidification processes*, J. Mater. Sci. **39** (2004), pp. 7285–7294.

[4] P. Rudolph, *Travelling magnetic fields applied to bulk crystal growth from the melt: The step from basic research to industrial scale*, J. Crystal Growth **310** (2008), pp. 1298–1306.

[5] P. Rudolph, C. Frank-Rotsch, F.-M. Kiessling, W. Miller, U. Rehse, O. Klein, C. Lechner, J. Sprekels, B. Nacke, H. Kasjanow, P. Lange, M. Ziem, B. Lux, M. Czupalla, O. Root, V. Trautmann, and G. Bethin, *Crystal growth in heater-magnet modules - from concept to use*, in Modelling for Electromagnetic Processing, 2008.

[6] J. Fainberg, D. Vizman, J. Friedrich, and G. Mueller, *A new hybrid method for the global modeling of convection in CZ crystal growth configurations*, J. Crystal Growth **303** (2007), pp. 124–134.

Authors

N. Dropka, Ch. Frank-Rotsch, W. Miller, U. Rehse, P. Rudolph
Leibniz Institute for Crystal Growth (IKZ),
Max-Born-Str.2, 12489 Berlin, Germany
E-Mail: dropka@ikz-berlin.de, miller@ikz-berlin.de, rehse@ikz-berlin.de, rudolph@ikz-berlin.de